



Article

Quantifying the Variation in Reflectance Spectra of Metrosideros polymorpha Canopies across Environmental Gradients

Megan M. Seeley ^{1,2,*}, Roberta E. Martin ^{1,2}, Nicholas R. Vaughn ¹, David R. Thompson ³, Jie Dai ¹ and Gregory P. Asner ^{1,2}

- Center for Global Discovery and Conservation Science, Arizona State University, Tempe, AZ 85281, USA
- School of Geographic Sciences and Urban Planning, Arizona State University, Tempe, AZ 85281, USA
- Jet Propulsion Laboratory, California Institute of Technology, 4800 Oak Grove Dr., Pasadena, CA 91109, USA
- * Correspondence: mseeley1@asu.edu

Abstract: Imaging spectroscopy is a burgeoning tool for understanding ecosystem functioning on large spatial scales, yet the application of this technology to assess intra-specific trait variation across environmental gradients has been poorly tested. Selection of specific genotypes via environmental filtering plays an important role in driving trait variation and thus functional diversity across space and time, but the relative contributions of intra-specific trait variation and species turnover are still unclear. To address this issue, we quantified the variation in reflectance spectra within and between six uniform stands of Metrosideros polymorpha across elevation and soil substrate age gradients on Hawai'i Island. Airborne imaging spectroscopy and light detection and ranging (LiDAR) data were merged to capture and isolate sunlit portions of canopies at the six M. polymorpha-dominated sites. Both intra-site and inter-site spectral variations were quantified using several analyses. A support vector machine (SVM) model revealed that each site was spectrally distinct, while Euclidean distances between site centroids in principal components (PC) space indicated that elevation and soil substrate age drive the separation of canopy spectra between sites. Coefficients of variation among spectra, as well as the intrinsic spectral dimensionality of the data, demonstrated the hierarchical effect of soil substrate age, followed by elevation, in determining intra-site variation. Assessments based on leaf trait data estimated from canopy reflectance resulted in similar patterns of separation among sites in the PC space and distinction among sites in the SVM model. Using a highly polymorphic species, we demonstrated that canopy reflectance follows known ecological principles of community turnover and thus how spectral remote sensing addresses forest community assembly on large spatial scales.

Keywords: imaging spectroscopy; leaf traits; environmental filtering; community assembly; environmental gradient; *Metrosideros polymorpha*



Citation: Seeley, M.M.; Martin, R.E.; Vaughn, N.R.; Thompson, D.R.; Dai, J.; Asner, G.P. Quantifying the Variation in Reflectance Spectra of *Metrosideros polymorpha* Canopies across Environmental Gradients. *Remote Sens.* 2023, 15, 1614. https://doi.org/10.3390/rs15061614

Academic Editor: Henning Buddenbaum

Received: 5 January 2023 Revised: 28 February 2023 Accepted: 13 March 2023 Published: 16 March 2023



Copyright: © 2023 by the authors. Licensee MDPI, Basel, Switzerland. This article is an open access article distributed under the terms and conditions of the Creative Commons Attribution (CC BY) license (https://creativecommons.org/licenses/by/4.0/).

1. Introduction

The spatial distribution of plant species has long been of interest to ecologists. Abiotic conditions constrain variations in species traits observed at a particular location via environmental filtering [1,2], and biotic competition further selects for specific traits [3]. Understanding how plant community assembly responds to shifts in environmental conditions on landscape scales is important for predicting and understanding community responses to climate change, species invasions, successional turnover, and functional diversity [4–7].

While theories of community assembly emphasize the importance of inter-specific competition and environmental filtering [1,7,8], the relative influence of these conditions in determining community composition is difficult to disentangle. The lack of emphasis on intra-specific, relative to inter-specific, trait variation has been called into question, especially with regard to the applicability of the leaf economic spectrum (LES) [9–11]. The LES describes correlations and trade-offs between leaf traits, specifically photosynthesis, leaf

Remote Sens. 2023, 15, 1614 2 of 18

nitrogen, and specific leaf area, as well as how these traits covary across environmental gradients [12–14]. Most LES studies, however, include multiple species, despite the recognized importance of intra-specific variation in overall trait variation [11,15,16]. In addition, many studies that have examined intra-specific trait variation studied individuals in common gardens or greenhouses and are focused at the leaf level [15,16]. Few studies exist that have examined how leaf traits vary across environmental gradients within a single species at the canopy level [10], yet quantifying how environmental filtering affects leaf traits in a single species is important for understanding how the functioning of a species varies spatially, especially those that dominate broad ecological niches.

Airborne imaging spectroscopy, a type of passive remote sensing data that quantifies reflected solar radiation, is ideal for addressing these questions. These data capture information about surface properties and can be used to estimate plant properties over wide areas [17], thereby advancing our understanding of forest functional ecology on large spatial scales [18–20]. Continued advances in imaging spectroscopy have allowed canopy traits to be quantified at high spatial resolution (2 m \times 2 m) [17,21,22]. By capturing a continuous portion of the electromagnetic spectrum from visible to short-wave infrared (SWIR; 400–2500 nm), imaging spectroscopy has been used to quantify canopy functional traits, including nitrogen, leaf mass per area, phenolics, and proteins, among others [22–25]. Some studies have demonstrated the potential of reflectance data alone for understanding forest ecology [18,19], while other studies have used reflectance-derived canopy functional traits, permitting the interpretation of the results through well-known environment–trait relationships, such as the LES [26]. However, distilling the electromagnetic spectrum into a handful of traits can also result in information loss [27].

Questions related to the relative information gained from canopy reflectance versus trait data and the intra-specific variation within a single species can be addressed by applying modern remote sensing technologies to Metrosideros polymorpha (ōhi'a) on Hawai'i Island. M. polymorpha is a model woody plant species with a biogeography and evolutionary history that make it ideal to study intra-specific trait responses to environmental filters [28]. M. polymorpha dominates native forests across the main Hawaiian Islands and often forms monodominant stands. Genetic variation across Metrosideros in Hawaii is largely due to migration into, and adaptation to, diverse abiotic conditions, especially elevation and soil substrate age [29,30]. Both elevation and soil substrate age affect growing conditions. For example, sites with young soils are nitrogen limited, while sites on the older end of the soil substrate age spectrum are phosphorus limited [31–33]. Furthermore, higher temperatures at low elevation sites affect not only nutrient accumulation in soils but also result in more optimal growing conditions than those found at high elevation sites [31]. At least four genetic varieties of this species self-sort on Hawai'i Island according to soil substrate age and elevation. While the different varieties can coexist and hybridize, monodominant stands of one variety are often common, especially at elevational extremes [34–36]. These unique properties of M. polymorpha make it a useful case study of environmental influence on intraspecies trait variation.

Much is known about canopy trait spatial distribution of this well-studied species [37–39], but no prior study has examined the *spectral* variation of *M. polymorpha* across environmental gradients using the full spectrum (400–2500 nm). Heritable differences in morphology, physiology, chemical traits, and spectral indices (e.g., green-red ratio, photochemical reflectance index) of *M. polymorpha* have been observed across elevation and soil substrate age gradients [37–42]. To capture the variation in reflectance spectra, hereafter referred to as spectral variation, of *M. polymorpha* canopies across elevation and soil substrate age gradients, we used six previously established sites on Hawai'i Island. These sites were used to answer the following questions:

- In a tropical/sub-tropical environment, do canopy spectra reflect the environmental filtering, and thus evolutionary divergence, of canopy properties in a single species?
- 2. How does the spectral variability of *M. polymorpha* capture the environmental filtering of traits across these environmental gradients in the context of the LES?

Remote Sens. 2023, 15, 1614 3 of 18

3. What is the relative performance of models using canopy spectra versus leaf trait indices estimated from reflectance data in differentiating the effects of environmental filtering on a single species?

The first question was addressed by quantifying the spectral variation of M. polymorpha at the canopy level across elevation and soil substrate age gradients. Because M. polymorpha varieties are filtered spatially by these environmental variables [30,43–45] and imaging spectroscopy captures heritable traits in M. polymorpha [16], as well as those in other species [46–48], we predicted that canopy spectra would differ across six sites representing different soil substrate age-elevation combinations. For the second question, inter-site variation was characterized relative to intra-site variation with respect to spectral characteristics and canopy traits. We predicted that estimated leaf indices would follow the LES, driving inter-site variations in the reflectance spectra. Furthermore, we expected that sites with less optimal growing conditions, whether caused by elevation or nutrient limitations, would restrict intra-site variation. As a result, the site at low elevation and with medium soil substrate age would have the greatest intra-site variation. To address the third question, we compared the performance of canopy reflectance versus canopy foliar traits to differentiate and describe the six sites. As canopy reflectance captures not only canopy traits but also their relative abundance and structure within the leaf and canopy, we expected that reflectance spectra would outperform estimated trait indices at differentiating the six sites.

2. Materials and Methods

2.1. Study Sites

Six nearly homogenous stands of *M. polymorpha* on the windward side of Hawai'i Island were selected for this investigation (Figure 1). We selected sites to control for top-of-canopy tree composition by focusing on areas with >90% *M. polymorpha* cover. The sites span elevation (200–1500 m) and soil substrate age (<200–500,000 years old) gradients (Table 1). Three soil substrate ages were represented (young, Y, medium, M, and old, O), and two sites, one at a higher elevation and one at a lower elevation (H and L, respectively), were selected for each soil substrate age. The largest stand (ML) was 53 ha, while the smallest (OL) was 8 ha.

Table 1. Descriptions of the six study sites. Data on soil age ranges were extracted from the U.S. Geological Survey [49] and the mean elevation for each site was calculated using the NASA Shuttle Radar Topography Mission (SRTM, 2013). The elevation difference for old soil substrate age sites was less than that of the other age categories due to constraints in the location of *M. polymorpha*-dominant stands. The maximum top of canopy height (TCH) was extracted from the LiDAR-derived TCH data. The normalized difference vegetation index (NDVI) was calculated using the 650 and 860 nm channels of the Global Airborne Observatory (GAO) reflectance data. The site mean percent nitrogen (N) and leaf mass per area (LMA) were calculated from geospatial leaf trait data estimated from GAO reflectance data using algorithms from Asner et al. [17].

Site	Description (Substrate Age, Elevation)	Area (ha)	Substrate Age Range (Years)	Mean Elevation (m)	TCH Max (m)	Mean NDVI	Mean LMA (g/m²)	Mean % N
YL	Young, Low	9	200-750	200	34	0.75	199.5	1.03
YH	Young, High	11	<200	1200	32	0.77	271.4	0.73
ML	Medium, Low	53	5000-11,000	750	36	0.85	198.1	1.80
MH	Medium, High	49	5000-64,000	1500	34	0.75	290.6	1.33
OL	Old, Low	8	260,000-500,000	900	10	0.85	196.2	0.54
OH	Old, High	10	260,000–500,000	1100	16	0.87	248.0	0.85

Remote Sens. 2023, 15, 1614 4 of 18

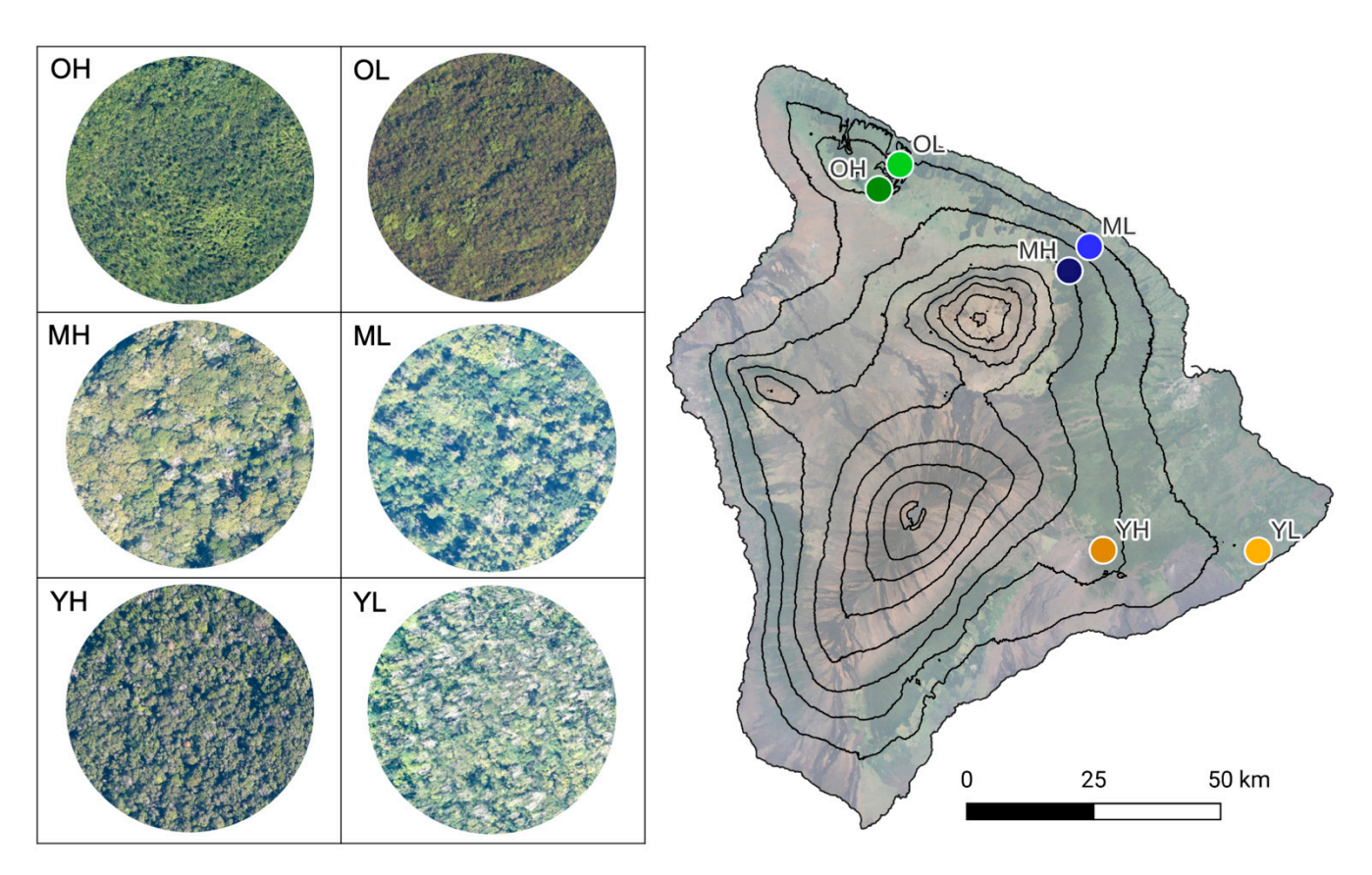


Figure 1. Global Airborne Observatory (GAO) Digital Modular Aerial Camera (DiMAC) imagery of the six study sites in red, green, and blue (true color) composites (**left**). Locations of the sites on Hawai'i Island (**right**). The sites are located along soil substrate age (Y, young <200–750; M, medium 5000–64,000; O, old 260,000–500,000) and elevation (L, low 200–900 m; H, high 1100–1500 m) gradients. See Table 1 for a summary of site information. Note that the DiMAC imagery shown here as a high-resolution reference to site conditions was not used in the analyses. Instead, see Figure S1 for GAO imaging spectroscopy true color composites of sites.

2.2. Data Processing

In January 2019, imaging spectroscopy data were collected by the Global Airborne Observatory (GAO) [50]. The GAO includes a high-fidelity imaging spectrometer (380–2510 nm) with a boresight-aligned dual-laser light detection and ranging (LiDAR) scanner. VSWIR data were orthorectified to 2 m × 2 m spatial resolution using precise time-synced position and orientation data from LiDAR and a surface elevation map generated from the first returns in the LiDAR data. Raw VSWIR data were converted to radiance using current spectral calibration and then processed to correct for atmospheric effects and retrieve hemispherical-direction reflectance values using ACORN v6.0 (Atmospheric CORrection Now; AIG LLC; Boulder, CO, USA) [51,52] and convolved from 5 nm to 10 nm bandwidth. VSWIR reflectance data from each of the six sites were then filtered to remove pixels representing understory vegetation, tree and cloud shadows, and non-photosynthetic vegetation. Top-of-canopy height (TCH) surface maps generated from LiDAR (Figure 2) were used to remove vegetation below two meters. Shaded pixels were removed using a shade mask generated using a ray tracing technique on the LiDAR-derived surface elevation map [50,53]. Lastly, non-photosynthetic vegetation was removed using a normalized difference vegetation index (NDVI) threshold of 0.7. This threshold was chosen based on a priori knowledge of the system to select pixels with intact and representative canopies. The NDVI data were generated using the 650 and 860 nm wavelengths of the VSWIR data. After filtering, 56% and 67% of the pixels in the YL and YH sites, respectively, remained. Fifty-four percent and 67% of the ML and MH pixels were retained, and the old soil substrate sites had the least

Remote Sens. 2023, 15, 1614 5 of 18

amount of filtering, with 93% and 96% of the site pixels remaining for the OL and OH sites, respectively (Table S1; Figure S1). This filtering process parallels the practice of collecting sunlit leaves near the top of the canopy for spectral or chemical analysis and reduces noise in the resulting signal.

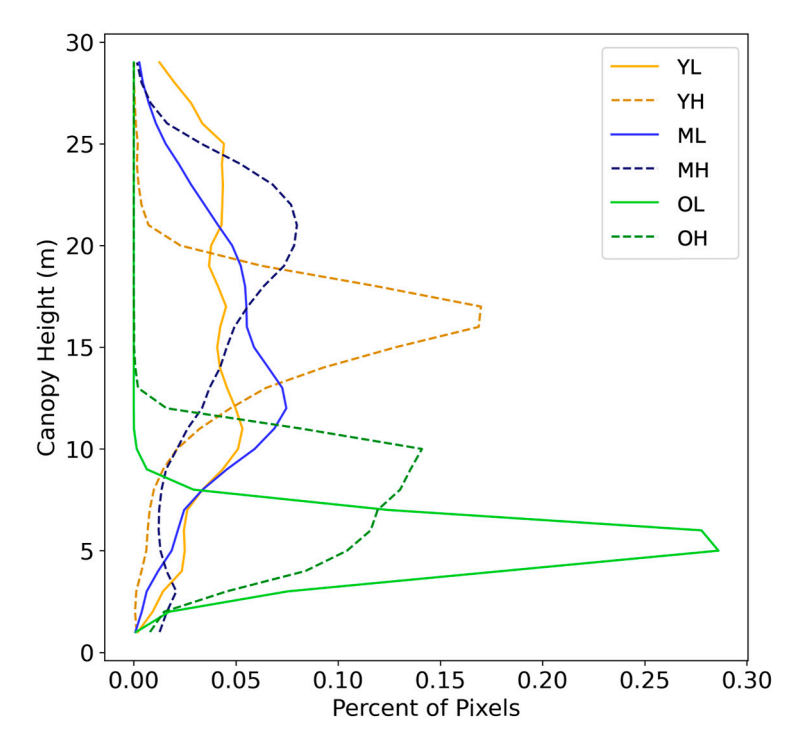


Figure 2. Top of canopy height (TCH) histogram showing the structural diversity of the six sites. Sites were characterized by soil substrate age (young, medium, or old) and elevation (low or high). TCH was derived from the unfiltered light detection and ranging (LiDAR) data collected by the Global Airborne Observatory. Sites are located along soil substrate age (Y, young <200–750; M, medium 5000–64,000; O, old 260,000–500,000) and elevation (L, low 200–900 m; H, high 1100–1500 m) gradients.

After filtering, the reflectance of the sunlit portion of the canopy was brightness normalized, converted to leaf traits, and subset to control for site size. Brightness normalization controls for variation in reflectance caused by subpixel shade, leaf volume, and leaf orientation relative to viewing and sun angles, thus minimizing the spectral variation not directly related to foliar chemistry [54]. To normalize the data, each VSWIR channel was divided by the vector norm of the entire VSWIR spectrum on a per-pixel basis. Nine canopy foliar traits (Table 2) were mapped from the brightness-normalized reflectance data using algorithms developed by Asner et al. [17]. We highlighted leaf mass per area (LMA) and percent foliar nitrogen (N) due to their importance in LES theory. For all analyses, we controlled for differences in site size by either randomly selecting a subset of pixels from each site (pixel-controlled method) or cropping each site to a 186 m × 186 m area (area-controlled method). For the pixel-controlled method, 12,997 pixels were randomly selected from all sites, as this was the number of pixels remaining after filtering in the smallest site (YL; Table S1). All pixels from the YL site were used. As the chemometric conversions included minimum and maximum brightness thresholds, the estimated leaf trait dataset had additional filtering and fewer remaining pixels (Table S1). As a result, 7474 pixels were randomly selected from the estimated trait datasets for each site, with all pixels from YH, the site with the fewest remaining pixels in the estimated leaf trait dataset, used in the analyses. For the area-controlled method, a 186 m \times 186 m extent was chosen, as it was the largest square we could crop from all sites based on their geometry.

Remote Sens. 2023, 15, 1614 6 of 18

Table 2. Canopy foliar traits estimated from GAO reflectance data using algorithms from Asner et al. (2015). See supporting information Figure S3 for site-level distributions of canopy traits.

Chemistry	Abbreviation	Units
Nitrogen	N	%
Leaf mass per area	LMA	${ m g}{ m m}^{-2}$
Chlorophyll	Chl	$ m g~m^{-2}$ $ m mg~g^{-1}$
Carotenoids	Car	$\mathrm{mg}\mathrm{g}^{-1}$
Phosphorus	P	%
Iron	Fe	$\mu \mathrm{g}~\mathrm{g}^{-1}$
Calcium	Ca	%
Total Carbon	Tot C	%
Soluble Carbon	Sol C	%

2.3. Analysis

Several analyses utilizing the reflectance values of independent bands or incorporating the correlations among bands were undertaken to explore the spectral diversity and separability of the six *M. polymorpha* stands (Table 3). We first examined inter-site and intra-site variation by plotting mean reflectance, mean brightness-normalized (BN) reflectance spectra, and the coefficient of variation (CV) per band of the BN reflectance for each of the sites. For these analyses, data were subset using the pixel-controlled method. Leaf traits are represented by the relative brightness of specific wavelength regions [55], so by comparing the mean reflectance of each site throughout the spectrum, we were able to qualitatively assess the relative foliar traits at each site. For example, the visible portion of the spectra (~400–700 nm) was used to quantify plant pigments, while short-wave infrared (SWIR; 1300–2500 nm) was important in quantifying other foliar traits, such as nitrogen, starch, and protein content [56]. We used the CV to describe the variability among spectra, as it is often applied to imaging spectroscopy data as a proxy for biodiversity [57].

Table 3. List of analyses performed on the data and their purposes in either directly addressing the research questions or as inputs in other analyses.

Method	Purpose			
Mean Brightness-Normalized Reflectance	 Assess inter-site variation across reflectance spectrum Qualitatively draw inferences about the sites based on their reflectance Standardize reflectance data across all sites 			
Coefficient of Variation	 Assess intra-site variation across reflectance spectrum Qualitatively draw inferences about the sites based on the variance of their reflectance 			
Principal Component Analysis (PCA)	 Reduce dimensionality of the dataset Used as input for calculating the intrinsic spectral dimensionality, Euclidean distance, and as training data for the SVM 			
Intrinsic Spectral Dimensionality	 Assess intra-site spectral variation across space Determine the number of PCs with meaningful spectral information to use in Euclidean distance measurements and in training the SVM 			
Euclidean Distance	 Quantify the distance (in the PC space) between sites as an estimation of site similarity Compare how sites separate when using reflectance data versus leaf trait data in PCA 			
Support Vector Machine (SVM)	 Assess the separability of the six sites (i.e., are they distinct?) Compare the relative performance of canopy spectra versus estimated trait indices in separating the six sites 			

To reorganize the highly dimensional spectral dataset (176 channels) into a hierarchical dataset in which the greatest variability is captured in the first principal component (PC), we employed principal component analysis (PCA). PCA is a powerful tool for exploring

Remote Sens. 2023, 15, 1614 7 of 18

imaging spectroscopy data because it describes the primary axes of spectral variability, even when these trends are correlated across multiple channels [58–60]. PCA reduces the dimensionality of data through eigen decomposition of the covariance matrix, where each subsequent PC captures less variability and is orthogonal, or uncorrelated, to the prior PC (Table S2) [50,60]. As PCA analyses are sensitive to the relative sample size in each category, we used the pixel-controlled method to calculate the PCs. PCA was applied to reflectance data from each site separately, as well as to both reflectance and leaf trait estimations from all sites. Results from the PCA analysis were used to calculate the intrinsic spectral dimensionality, Euclidean distance, and as training data for the support vector machine (SVM), as described below.

To evaluate the spectral diversity of the six M. polymorpha-dominated sites, we calculated their intrinsic spectral dimensionality, a proxy for surface property diversity [58,61]. Intrinsic spectral dimensionality measures the observable degrees of freedom—meaningful information at each site—by estimating the number of principal components derived from the reflectance data that have a significant spatially coherent signal [58]. The intrinsic spectral dimensionality was calculated following the procedure of Thompson et al. [58]. PCs from PCA applied to each site separately (local PCA) and to all site data (global PCA) were mapped across the 186 m × 186 m subset of their respective sites (areacontrolled method). To determine the intrinsic spectral dimensionality of all sites, PC data from the upper left 62 m × 94 m of each site were combined into a pseudo-site (186 m \times 188 m), with data from each site remaining intact spatially. The arrangement of site data within the pseudo-site matrix, as well as the size of each site within the matrix, did not affect the results. Next, we created "signal" images by smoothing all spatial PC data with a 3 × 3 pixel averaging kernel. "Noise" images were developed by subtracting the signal image from the original PC image. To determine the magnitude of the signal and noise for each PC, we calculated the standard deviation of each and identified the first PC, sorted by decreasing eigenvalues, where the magnitude of the signal was less than that of noise. As the precise crossover point—where noise exceeded signal—can be unstable for small dataset sizes, we determined intrinsic spectral dimensionality using the first of three sequential PCs, where the magnitude of the signal was less than that of noise. We found that the intrinsic spectral dimensionality of the global dataset (all the sites combined into the pseudo-site) was 16. As the first 16 PCs contained meaningful spatial information in feature space, we used the first 16 PCs derived from the reflectance data in the subsequent analyses (see Table S2 for PC loadings).

To understand the relative separability of the six sites with regard to their elevation—soil substrate age combination, site centroids were projected onto a 2D space based on their Euclidean distance in the PC space. PCA-transformed reflectance and estimated leaf trait data were used to identify site centroids by calculating site means along each of the first 16 PCs for the reflectance data and along each of the 9 estimated leaf trait PCs. Next, the Euclidean distance, defined as the shortest distance between two points in n-dimensional space, was calculated for each site combination. These distances were projected into 2D space, allowing us to assess the separation or clustering of sites based on their reflectance or estimated trait data.

To determine whether the reflectance data and the estimated leaf trait data from each site were unique, we employed an SVM. SVMs, typically nonlinear supervised classifiers, are commonly used in imaging spectroscopy applications, as they can efficiently handle highly dimensional datasets, and the results are relatively straightforward to interpret compared to more complicated machine learning algorithms [62–66]. SVM classifiers create decision boundaries between two categories in feature space by maximizing the distance between the decision boundary and the training data [67]. While SVMs are typically used to create general-purpose classifiers, here we used an SVM to assess whether the distributions of the spectra from the six sites were separable. We used the first 16 PCs of the reflectance data to reduce the dimensionality of the dataset. Because applying an SVM to all PC bands is equivalent to training the model on the untransformed dataset, estimated leaf

Remote Sens. 2023, 15, 1614 8 of 18

trait data with no PCA transformation were used as training input. To reduce the effect of spatial autocorrelation in selecting the test and training datasets, the data, randomly subset according to the pixel-controlled method, were further subset into northern and southern sections, with 1/3 of the northernmost pixels used as test data and the southernmost 2/3 of the pixels used for training. Next, an SVM with cross validation to optimize hyperparameter selection was fit to the two datasets using the scikit-learn package (version 0.24.1) in Python (version 3.6.9) [68]. The SVM parameters included a radial basis function kernel and a grid search to optimize the kernel coefficient and regulation parameters.

3. Results

Inter-site spectral variation primarily followed elevational gradients, while intrasite spectral variation was primarily driven by soil substrate age, as demonstrated by the CV, intrinsic spectral dimensionality, and Euclidean distances. Inter-site variation in canopy reflectance and estimated leaf traits led to high classification accuracies for the SVM. Estimated leaf trait information supported and helped explain the results obtained from reflectance data alone.

3.1. Inter-Site Variation

We compared the mean spectra of the six sites using both non-normalized and brightness-normalized spectra (Figure 3). Brightness normalization preserves variations in spectral shape and minimizes differences in overall spectral brightness. Comparing mean site spectra, reflectance variability in the range of the 1200 nm water feature was reduced following brightness normalization, while variation in the shortwave-infrared (>1300 nm) and visible (<700 nm) portions of the spectrum expanded (Figure 3a,b). In the normalized SWIR region, the mean spectra of the high elevation sites converged, and between 2000–2500 nm, the YL and OL sites likewise converged (Figure 3b). The ML site had the lowest values in the SWIR relative to all the other sites, whereas the YL and OL sites exceeded the other sites in the SWIR. ML and OL had the lowest green peak (~550) in the normalized reflectance, while YL, MH, and OH had the highest.

Through the SVM classifier, we found that inter-site spectral variation exceeded intrastite variation (Table 4). The SVM was trained using PCs 1-16, based on the calculation of intrinsic dimensionality of all sites combined. The accuracy and precision of this model were 0.998 for both. According to the confusion matrix, the OL site was the most distinct, as the SVM was the most accurate for this site (100%; Table 4). While the SVM demonstrated high accuracy across the sites, ML and OH had the lowest accuracies. Pixels from high and low elevations on the medium substrate age were confused (0.2% combined), while the high and low sites on the other substrate ages were not. YL was one of the only sites misclassified as another site of similar elevation (ML), and MH was only confounded with a site of similar soil substrate age (ML) or elevation (OH). YH misclassifications into other sites were less than one percent, and OH was confounded with the medium soil substrate age sites.

The relative importance of elevation versus soil substrate age on inter-site variability was assessed using Euclidean distance measures between centroids of each site in the PC space calculated from the global dataset (Figure 4; Table S3). Distances between site centroids were mapped for PCs 1-16. Similar to the pattern observed in the mean brightness-normalized SWIR, the ML site centroid was furthest from the other low elevation sites, whereas the YL and OL centroids were close to each other in the PC space. The high sites were clustered relative to the other sites, with OH and MH being the closest of all the site centroids. The MH and ML site centroids were the second-closest pair in the PC space.

Remote Sens. 2023, 15, 1614 9 of 18

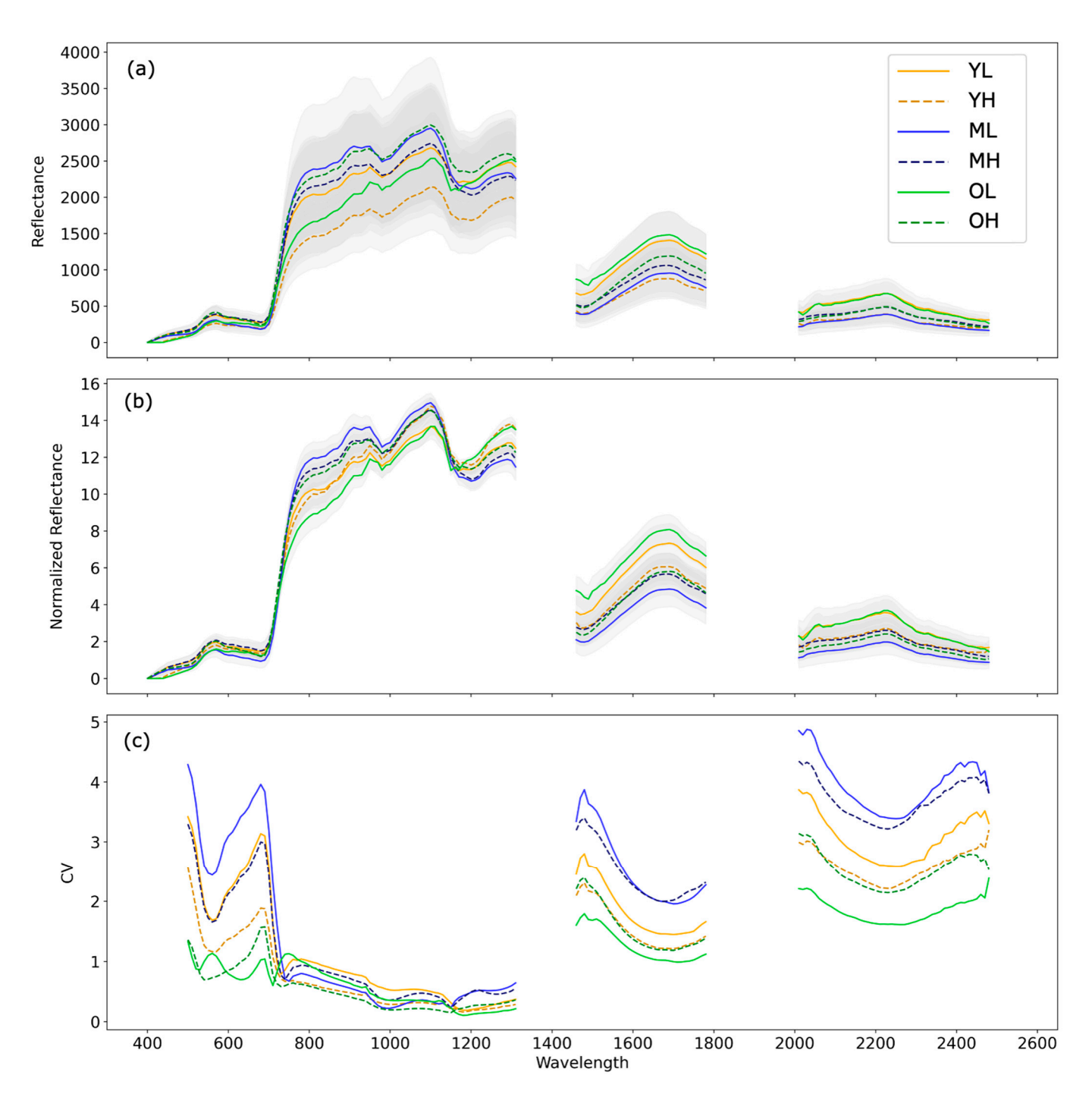


Figure 3. Mean and standard deviation (gray fill) (a) reflectance and (b) brightness-normalized reflectance for the six sites. See Figure S2 for brightness normalized reflectance of each site plotted individually. (c) Coefficient of variation (CV) of brightness-normalized reflectance for all sites. Site data were subset to control for the number of pixels included in each site (pixel-controlled method). Sites are located along soil substrate age (Y, young <200–750; M, medium 5000–64,000; O, old 260,000–500,000) and elevation (L, low 200–900 m; H, high 1100–1500 m) gradients.

Remote Sens. 2023, 15, 1614 10 of 18

Table 4. Confusion matrix of the support vector machine (SVM) with radial basis function kernel applied to the first 16 principal components calculated from reflectance data. Values are presented as the percentage of pixels predicted into each class. Site acronyms indicate soil substrate age (Y, young <200–750; M, medium 5000–64,000; O, old 260,000–500,000) and elevation (L, low 200–900 m; H, high 1100–1500 m).

		Predicted					
		YL	YH	ML	MH	OL	ОН
	YL	99.8	0	0	0.1	0	0
	ΥH	0	99.9	0	0	0	0
1	ML	0.2	0	99.6	0.1	0	0.2
Actual	MH	0.1	0	0.1	99.7	0	0.1
	OL	0	0	0	0	100	0
	OH	0	0	0.3	0.2	0	99.6

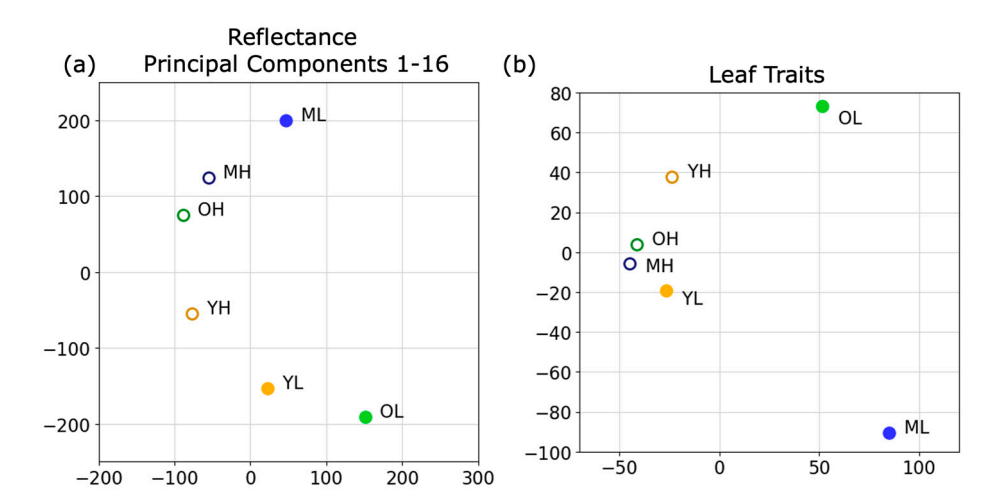


Figure 4. Euclidean distances between the centroid of each site projected onto 2D space. The Euclidean distance was calculated using (a) the first 16 principal components (PCs) of the reflectance data and (b) the nine PCs of leaf traits. See Table 2 for a list of the leaf traits included. See Table S3 for the distances between sites. Sites are located along soil substrate age (Y, young <200–750; M, medium 5000–64,000; O, old 260,000–500,000) and elevation (L, low 200–900 m; H, high 1100–1500 m) gradients.

3.2. Intra-Site Variation

The CV of the spectra suggest that *M. polymorpha* stands, as observed through their spectra, were responsive to either soil substrate age or, to a lesser extent, elevation (Figure 3c). In the SWIR region, the CV of medium soil substrate age sites was largest, followed by young sites. For young and medium sites, intra-site variation in the SWIR was lower at high elevations than at lower elevations. The opposite pattern was observed in old soil substrate age sites, and this was attributed to the OL site being on an eroded shield of higher than expected nutrient concentration [69]. In the visible portion of the spectrum, a similar pattern in relative variance between the sites was observed, except for the convergence of MH and YL. Furthermore, the OL CV peaked around the green wavelengths (~550 nm), causing the shape of the OL CV to diverge from that of the other sites, as they displayed a local minimum in the green wavelengths.

The intrinsic spectral dimensionality of each site further suggests the primary importance of soil substrate age, followed by elevation, in determining intra-site variability (Figure 5). The intrinsic spectral dimensionality calculated using local and global PCAs yielded similar, though not identical, patterns of intra-site variability. For both local and global PCA, the medium elevation sites had the highest intra-site variation. The global PCA followed a similar hierarchy in intra-site variability as the CV, where low elevation sites had higher intrinsic spectral dimensionality than high elevation sites on young- and medium-

Remote Sens. 2023, 15, 1614 11 of 18

aged lava flows; however, the difference between elevations was smaller for young sites. This elevational pattern was again reversed for the old soil substrate age sites. For local PCA, no elevation patterns were observed for the medium soil substrate age sites, and the OL site had greater intrinsic spectral dimensionality than the OH site (Figure 5).

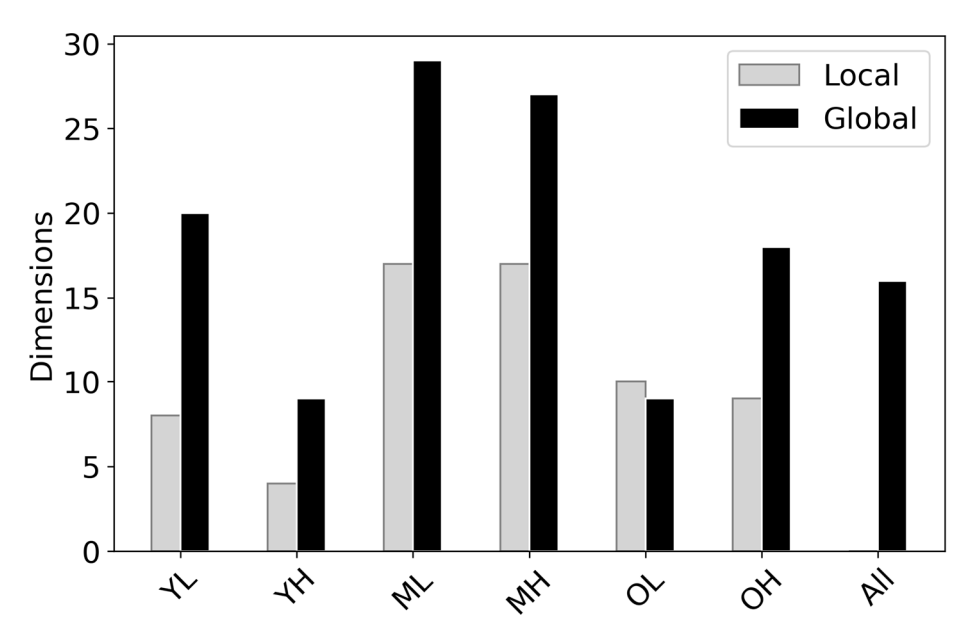


Figure 5. The intrinsic spectral dimensionality of each site calculated using both local (gray) and global (black) principal component analyses (PCA) applied to the filtered reflectance data. The areal extent of each site was controlled (area-controlled method) such that the area of each site used in the analysis was equivalent. The global intrinsic spectral dimensionality (calculated across all sites) is represented by the "All" category. Sites are located along soil substrate age (Y, young <200–750; M, medium 5000–64,000; O, old 260,000–500,000) and elevation (L, low 200–900 m; H, high 1100–1500 m) gradients.

3.3. Canopy Traits

Canopy chemistries were calculated to compare reflectance versus trait data in their ability to differentiate and describe the six sites, as well as place the results derived from the reflectance data into the context of well-described ecological patterns. In the PC space, sites grouped similarly when Euclidean distances were calculated using reflectance and trait data (Figure 4). Similar to the reflectance data, the estimated leaf traits separated the sites based on elevation along one axis, and while MH and OH clustered, separation along one axis according to elevation was not as prominent as with the reflectance data. The OL and ML sites were the most distant from the other sites (Figure 4). The canopy trait variance was greatest at the ML site for nine out of the nine traits estimated, while OL had the lowest variance for nine out of the nine traits (Table S4). When comparing the ability of trait versus reflectance data to classify data into one of the six sites using an SVM, the SVM trained using the reflectance data outperformed that using the trait data. The accuracy and precision of the SVM trained using the nine chemistries were 0.912 and 0.913, respectively, which was similar to the SVM applied to the PCs of the reflectance data.

Dry leaf mass per area (LMA; g m⁻²) and percent nitrogen (N) followed known patterns of leaf traits along ecological gradients (Figure 6). Foliar N estimated for the six sites fell within the range of a forested elevation gradient on the windward side of Hawai'i Island presented by Balzotti and Asner [70]. Foliar N was highest on average for the ML site, followed by the MH site, and lowest for the OL site. The mean foliar N was higher on the low elevation than the high elevation sites for both young and medium soil substrate ages, while the OL site was lower in foliar N than on the OH site. We note that since the RMSE of foliar N, as presented by Asner et al. [17], is 0.31, differences between the

Remote Sens. 2023, 15, 1614 12 of 18

YL and YH as well as the OL and OH sites may be negligible. Mean foliar N patterns along the soil substrate age and elevation gradients, including low N in the OL site, follow the intra-site variation observed in the CV of the spectra. Patterns in LMA followed the elevation gradient, with high elevation sites displaying higher LMA than low elevation sites (Figure 6). Across all soil substrate ages, the high sites had approximately $70~{\rm g~m}^{-2}$ greater LMA than the low sites.

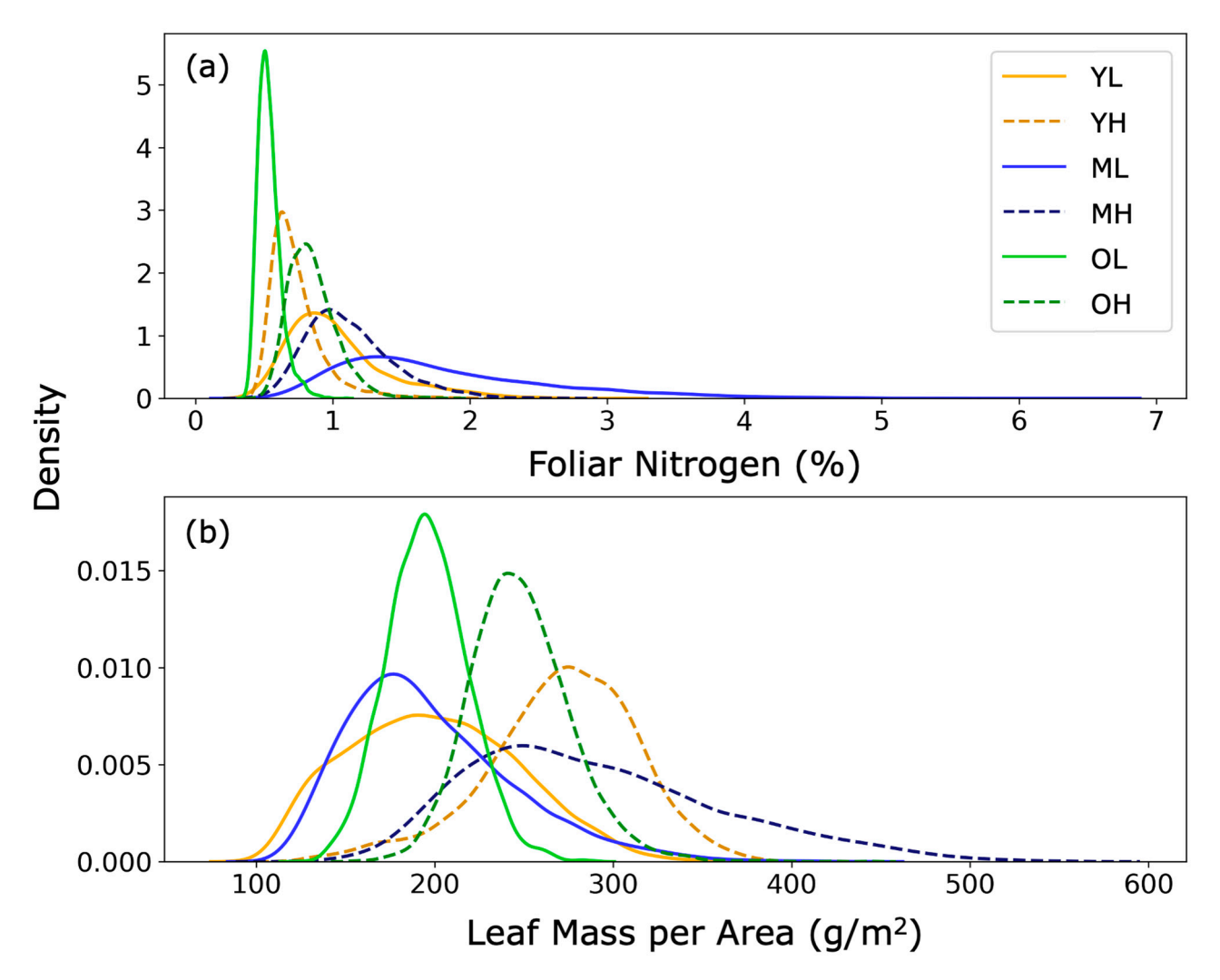


Figure 6. Distributions of modeled canopy chemistry indices for (a) foliar nitrogen (%) and (b) leaf mass per area (LMA; g m $^{-2}$) across each of the six sites. The total number of pixels used to create the site kernel density plots was equivalent to that at the smallest site and randomly selected from each site. Sites are located along soil substrate age (Y, young <200–750; M, medium 5000–64,000; O, old 260,000–500,000) and elevation (L, low 200–900 m; H, high 1100–1500 m) gradients. See supporting information in Figure S3 and Table S4 for the distributions of all canopy chemistries.

4. Discussion

The spectra of closed canopy *M. polymorpha* forests were compared to assess the effect of environmental filtering on the functioning of a single species. We found that the spectra of the six forest sites differed along soil substrate age and elevation gradients. These results are consistent with prior work describing heritable morphological differences between *M. polymorpha* populations at high and low elevations, as well as on lava flows of different ages [16,39,71–73].

Consistent with the leaf economic spectrum (LES), the LMA of *M. polymorpha* increased with increasing elevation [37,39], and these results are further supported by our LMA

Remote Sens. 2023, 15, 1614 13 of 18

estimates from canopy reflectance. LMA is a structural feature of leaves that is often used as an indicator of plant life strategies and functional groups, as it correlates with leaf nitrogen, proteins, and photosynthetic rate [74,75]. Plants with low LMA tend to exhibit higher growth rates, and their leaves tend to be more susceptible to damage and predation. High LMA leaves are often higher in secondary defense metabolites and are associated with lower growth rates [74,76]. The LMA of M. polymorpha has been reported to vary from <200 to >400 g m⁻² along an elevation gradient [41].

Other leaf traits, such as $\delta 13$ C, leaf-level spectra, foliar N, and other leaf chemical properties, differ among populations at different elevations and soil substrate ages, although the effect is often more pronounced along elevational gradients. A large variation in leaf N has been observed across M. polymorpha elevation gradients, with foliar N being three times greater at high versus low elevation sites [39]. Because N availability is related to soil development, older lava substrates have accumulated more N than younger flows, and, to a lesser extent, elevation is negatively related to soil N [77,78]. Furthermore, foliar N can be indicative of available soil N [28]. These adaptations to nutrient limitations, temperature, and precipitation along environmental gradients on Hawai'i Island have resulted in functional and genetic differentiation of M. polymorpha [30,79,80] and have now been observed through canopy-level spectra.

Inter-site variability was greatest across elevation gradients, as opposed to soil substrate age gradients, which supports other field-based work observing stronger phenological responses in *M. polymorpha* to elevation than soil substrate age [37,38]. Separation of mean reflectance in the brightness-normalized visible and SWIR indicate site-level differences in leaf chemistries. In the PC space, sites similar in elevation clustered, regardless of soil substrate age. The relative influence of climatic conditions was greater than the geologic patterns in driving canopy spectra, suggesting that anthropogenic climate change will likely have strong influences on the biogeography of *M. polymorpha*.

Site separability was demonstrated using an SVM and by calculating the Euclidean distances between the sites in the PC space of the reflectance data and modeled canopy traits. The SVM was able to classify each site with the reflectance data with high accuracy, indicating that canopy reflectance at each site was distinct. The differentiation of the site reflectance data is likely driven by the selection of different genotypes through environmental filtering. M. polymorpha phenological differences across environmental gradients [16,37–42] are heritable, as has been demonstrated in common garden experiments [16,39,40,81] and through DNA sequencing [30,34,35]. On Hawai'i Island, environmental filtering plays an important role in selecting for different genetic variants of M. polymorpha [30,43,45], and our SVM results demonstrated that canopy reflectance data can differentiate M. polymorpha from six stands representing environmental gradients that select for different M. polymorpha traits. We note that the SVM was used to determine the separability of the six sites, so model performance was not assessed on spatially independent sites. Furthermore, while we attribute most of the high accuracy and precision achieved by the SVM to differences in the M. polymorpha canopies among the sites, factors such as environmental, illumination, or atmospheric factors may have contributed to the model's performance. The dominance of M. polymorpha in the Hawaiian model system allows us to observe and understand intra-specific trait variation across environmental gradients, a type of "genetic turnover" akin to species turnover in most other systems.

While elevation was a stronger driver of inter-site variability, soil substrate age was the primary determinant of intra-site variability. The CV and intrinsic spectral dimensionality, both estimates of site-level diversity, demonstrate a clear hierarchical pattern of variation within each site, with intra-site variation organized first by soil substrate age and then by elevation. Sites on medium soil substrate age had greater intra-site variability than sites on young and old soil substrates. Site elevation was a secondary driver of intra-site variability, with low sites having more variability than high sites. The OL site was an exception to this pattern, which is likely a result of nutrient limitations at this site due to its presence on an eroded shield. Chronosequences across lava flows have demonstrated a

Remote Sens. 2023, 15, 1614 14 of 18

peak in foliar nitrogen and phosphorous found in *M. polymorpha* on sites of intermediate age [77]. Sites early in soil development are nitrogen limited, while older lava flows are characterized by phosphorous (P) limitations [44,77]. Foliar percent N estimated using the GAO reflectance data supports the conclusion that the medium-aged sites were richer in N than the other sites, as foliar N reflects available soil N [28]. Of the six sites, ML had the most optimal growing conditions, which was reflected in the high intra-site variability of both the canopy reflectance and trait indices. Intra-site variability of the six *M. polymorpha* sites, as observed through canopy reflectance, followed patterns of leaf trait variability across environmental gradients.

Imaging spectroscopy is a powerful tool for ecology, but whether reflectance data can be interpreted directly or converted into canopy traits is debated. Spectranomics, the field of interpreting reflectance data through plant traits, emerged because of the challenges involved in understanding spectra in the context of ecology [26]. The Hawai'i *M. polymorpha* model system has allowed us to not only demonstrate the potential of using spectra as a lens through which we can understand the evolution of a species across diverse ecological niches but also compare reflectance- and trait-based analyses. The SVM models and Euclidean distances between sites in the PC space were similar for both reflectance and trait data, leading to comparable interpretations of the results. Furthermore, as spectranomics is an important lens through which to understand reflectance data, it has the advantage of allowing us to interpret imaging spectroscopy data in the context of known ecological concepts.

5. Conclusions

This application of imaging spectroscopy data to a model system demonstrates the potential for canopy reflectance data to address forest community assembly on large spatial scales. As our study is limited to six sites, each representing a unique soil substrate age-elevation combination, we note that the lack of replication restricts our interpretation of the results. However, the patterns observed in these data follow known ecological principles, suggesting that future work can expand upon these results for a more rigorous statistical analysis of the environmental factors driving canopy reflectance patterns. The observed differences in reflectance spectra at the six sites are underpinned by variations in canopy leaf traits. The high spectral resolution of imaging spectroscopy has allowed canopy water content [82] and foliar traits, such as N, net primary productivity, and lignin [21,26,83], to be quantified from aircraft. We have demonstrated the ability to assess the intra-site and inter-site variability of canopy traits using canopy spectra and how spectral variability follows a well-known model system. By including both soil substrate age and elevation gradients, we demonstrated the dominant influence of soil substrate age on intra-site variation, while inter-site variation was primarily driven by elevation. In addition, we can see in the reflectance data how environmental filtering has resulted in "genetic turnover" of M. polymorpha in a manner similar to species turnover in more diverse regions. As imaging spectroscopy data become more widely available with the upcoming launch of spaceborne spectrometers, the ability to use these data to explore community assembly across even larger spatial scales will advance our understanding of forest functioning at a global level.

Supplementary Materials: The following supporting information can be downloaded at: https://www.mdpi.com/article/10.3390/rs15061614/s1, Table S1. The total number of 2 m pixels in each of the six sites, as well as the number of pixels remaining after filtering; Table S2. Principal component (PC) loadings for the first 16 PCs of the PCA applied to the reflectance data of all six sites (referred to as the global PCA); Table S3. Euclidean distance between the site centroids in the principal component (PC) space; Table S4. Mean and standard deviation (std) for each site of all nine chemistries estimated from reflectance spectra; Figure S1. Filtered red, green, and blue (true color) composites of the six sites; Figure S2: Mean and standard deviation (gray fill) brightness-normalized reflectance from Figure 3b, with each site separated for clarity; Figure S3. Kernel density estimates of canopy traits.

Remote Sens. 2023, 15, 1614 15 of 18

Author Contributions: Conceptualization, M.M.S. and G.P.A.; methodology, M.M.S., R.E.M., N.R.V., D.R.T., J.D. and G.P.A.; data curation, N.R.V.; formal analysis, M.M.S.; writing—original draft preparation, M.M.S.; writing—review and editing, all authors; funding acquisition, D.R.T. and G.P.A. All authors have read and agreed to the published version of the manuscript.

Funding: This research was funded by NASA grant SURP-2020-018 to G.A. and D.T. Scientist support was provided through an ASU Gilbert F. White Environment and Society Fellowship. A portion of the research was carried out at the Jet Propulsion Laboratory, California Institute of Technology, under a contract with the National Aeronautics and Space Administration (80NM0018D0004). The Global Airborne Observatory (GAO) is managed by the Center for Global Discovery and Conservation Science at Arizona State University. The GAO is made possible by support from private foundations, visionary individuals, and Arizona State University.

Data Availability Statement: The data presented in this study are openly available in Figshare at 10.6084/m9.figshare.22272670.

Conflicts of Interest: The authors declare no conflict of interest.

References

- 1. Weiher, E.; Clarke, G.D.P.; Keddy, P.A. Community Assembly Rules, Morphological Dispersion, and the Coexistence of Plant Species. *Oikos* 1998, *81*, 309–322. [CrossRef]
- 2. Keddy, P.A. Assembly and response rules: Two goals for predictive community ecology. J. Veg. Sci. 1992, 3, 157–164. [CrossRef]
- 3. Macarthur, R.; Levins, R. The Limiting Similarity, Convergence, and Divergence of Coexisting Species. *Am. Nat.* **1967**, *101*, 377–385. [CrossRef]
- 4. Morin, X.; Lechowicz, M. Contemporary perspectives on the niche that can improve models of species range shifts under climate change. *Biol. Lett.* **2003**, *4*, 573–576. [CrossRef]
- 5. Buzzard, V.; Hulshof, C.M.; Birt, T.; Violle, C.; Enquist, B.J. Re-growing a tropical dry forest: Functional plant trait composition and community assembly during succession. *Funct. Ecol.* **2016**, *30*, 1006–1013. [CrossRef]
- 6. Richardson, D.M.; Pyšek, P.; Rejmánek, M.; Barbour, M.G.; Panetta, F.D.; West, C.J. Naturalization and invasion of alien plants: Concepts and definitions. *Divers. Distrib.* **2000**, *6*, 93–107. [CrossRef]
- 7. Swenson, N.G.; Enquist, B.J.; Pither, J.; Kerkhoff, A.J.; Boyle, B.; Weiser, M.D.; Elser, J.J.; Fagan, W.F.; Forero-Montaña, J.; Fyllas, N.; et al. The biogeography and filtering of woody plant functional diversity in North and South America. *Glob. Ecol. Biogeogr.* **2012**, *21*, 798–808. [CrossRef]
- 8. Kraft, N.J.B.; Adler, P.B.; Godoy, O.; James, E.C.; Fuller, S.; Levine, J.M. Community assembly, coexistence and the environmental filtering metaphor. *Funct. Ecol.* **2015**, *29*, 592–599. [CrossRef]
- 9. Anderegg, L.D.L.; Berner, L.T.; Badgley, G.; Sethi, M.L.; Law, B.E.; HilleRisLambers, J. Within-species patterns challenge our understanding of the leaf economics spectrum. *Ecol. Lett.* **2018**, *21*, 734–744. [CrossRef]
- 10. Schneider, F.D.; Morsdorf, F.; Schmid, B.; Petchey, O.L.; Hueni, A.; Schimel, D.S.; Schaepman, M.E. Mapping functional diversity from remotely sensed morphological and physiological forest traits. *Nat. Commun.* **2017**, *8*, 1441. [CrossRef]
- 11. Albert, C.H.; Thuiller, W.; Yoccoz, N.G.; Soudant, A.; Boucher, F.; Saccone, P.; Lavorel, S. Intraspecific functional variability: Extent, structure and sources of variation. *J. Ecol.* **2010**, *98*, 604–613. [CrossRef]
- 12. Wright, I.J.; Reich, P.B.; Westoby, M.; Ackerly, D.D.; Baruch, Z.; Bongers, F.; Cavender-Bares, J.; Chapin, T.; Cornelissen, J.H.C.; Diemer, M.; et al. The worldwide leaf economics spectrum. *Nature* **2004**, *428*, 821–827. [CrossRef]
- 13. Read, Q.D.; Moorhead, L.C.; Swenson, N.G.; Bailey, J.K.; Sanders, N.J. Convergent effects of elevation on functional leaf traits within and among species. *Funct. Ecol.* **2014**, *28*, 37–45. [CrossRef]
- 14. Midolo, G.; De Frenne, P.; Hölzel, N.; Wellstein, C. Global patterns of intraspecific leaf trait responses to elevation. *Glob. Chang. Biol.* **2019**, 25, 2485–2498. [CrossRef] [PubMed]
- 15. Wright, J.P.; Sutton-Grier, A. Does the leaf economic spectrum hold within local species pools across varying environmental conditions? *Funct. Ecol.* **2012**, *26*, 1390–1398. [CrossRef]
- 16. Martin, R.E.; Asner, G.P.; Sack, L. Genetic variation in leaf pigment, optical and photosynthetic function among diverse phenotypes of *Metrosideros polymorpha* grown in a common garden. *Oecologia* **2007**, *151*, 387–400. [CrossRef]
- 17. Asner, G.P.; Martin, R.E.; Anderson, C.B.; Knapp, D.E. Quantifying forest canopy traits: Imaging spectroscopy versus field survey. *Remote Sens. Environ.* **2015**, *158*, 15–27. [CrossRef]
- 18. Draper, F.C.; Baraloto, C.; Brodrick, P.G.; Phillips, O.L.; Martinez, R.V.; Coronado, E.N.H.; Baker, T.R.; Gómez, R.Z.; Guerra, C.A.A.; Flores, M.; et al. Imaging spectroscopy predicts variable distance decay across contrasting Amazonian tree communities. *J. Ecol.* 2019, 107, 696–710. [CrossRef]
- Kalacska, M.; Sanchez-Azofeifa, G.A.; Rivard, B.; Caelli, T.; White, H.P.; Calvo-Alvarado, J.C. Ecological fingerprinting of ecosystem succession: Estimating secondary tropical dry forest structure and diversity using imaging spectroscopy. *Remote Sens. Environ.* 2007, 108, 82–96. [CrossRef]

Remote Sens. 2023, 15, 1614 16 of 18

20. DuBois, S.; Desai, A.R.; Singh, A.; Serbin, S.P.; Goulden, M.L.; Baldocchi, D.D.; Ma, S.; Oechel, W.C.; Wharton, S.; Kruger, E.L.; et al. Using imaging spectroscopy to detect variation in terrestrial ecosystem productivity across a water-stressed landscape. *Ecol. Appl.* **2018**, *28*, 1313–1324. [CrossRef]

- 21. Kokaly, R.F.; Asner, G.P.; Ollinger, S.V.; Martin, M.E.; Wessman, C.A. Characterizing canopy biochemistry from imaging spectroscopy and its application to ecosystem studies. *Remote Sens. Environ.* **2009**, *113*, S78–S91. [CrossRef]
- 22. Asner, G.P.; Martin, R.E.; Knapp, D.E.; Tupayachi, R.; Anderson, C.; Carranza, L.; Martinez, P.; Houcheime, M.; Sinca, F.; Weiss, P. Spectroscopy of canopy chemicals in humid tropical forests. *Remote Sens. Environ.* **2011**, *115*, 3587–3598. [CrossRef]
- 23. Asner, G.P.; Knapp, D.E.; Anderson, C.B.; Martin, R.E.; Vaughn, N. Large-scale climatic and geophysical controls on the leaf economics spectrum. *Proc. Natl. Acad. Sci. USA* **2016**, *113*, E4043–E4051. [CrossRef]
- 24. Wang, Z.; Chlus, A.; Geygan, R.; Ye, Z.; Zheng, T.; Singh, A.; Couture, J.J.; Cavender-Bares, J.; Kruger, E.L.; Townsend, P.A. Foliar functional traits from imaging spectroscopy across biomes in eastern North America. *New Phytol.* **2020**, 228, 494–511. [CrossRef] [PubMed]
- 25. Singh, A.; Serbin, S.P.; McNeil, B.E.; Kingdon, C.C.; Townsend, P.A. Imaging spectroscopy algorithms for mapping canopy foliar chemical and morphological traits and their uncertainties. *Ecol. Appl.* 2015, 25, 2180–2197. [CrossRef]
- 26. Asner, G.P.; Martin, R.E. Convergent elevation trends in canopy chemical traits of tropical forests. *Glob. Chang. Biol.* **2016**, 22, 2216–2227. [CrossRef]
- 27. Féret, J.-B.; Asner, G.P. Mapping tropical forest canopy diversity using high-fidelity imaging spectroscopy. *Ecol. Appl.* **2014**, 24, 1289–1296. [CrossRef] [PubMed]
- 28. Vitousek, P.M. Nutrient Cycling and Limitation: Hawai'i as a Model System; Princeton University Press: Princeton, NJ, USA, 2004.
- 29. Morrison, K.R.; Stacy, E.A. Intraspecific divergence and evolution of a life-history trade-off along a successional gradient in Hawaii's *Metrosideros polymorpha*. *J. Evol. Biol.* **2014**, 27, 1192–1204. [CrossRef] [PubMed]
- 30. Stacy, E.A.; Johansen, J.B.; Sakishima, T.; Price, D.K.; Pillon, Y. Incipient radiation within the dominant Hawaiian tree *Metrosideros polymorpha*. *Heredity* **2014**, 113, 334–342. [CrossRef]
- 31. Vitousek, P.M.; Aplet, G.; Turner, D.; Lockwood, J.J. The Mauna Loa environmental matrix: Foliar and soil nutrients. *Oecologia* **1992**, *89*, 372–382. [CrossRef]
- 32. Vitousek, P.M.; Chadwick, O.; Crews, T.E.; Fownes, J.; Hendricks, D.M.; Herbert, D. Soil and ecosystem development across the Hawaiian Islands. *GSA Today* **1997**, *7*, 1–8.
- 33. Herbert, D.A.; Fownes, J.H. Forest Productivity and Efficiency of Resource Use across a Chronosequence of Tropical Montane Soils. *Ecosystems* **1999**, *2*, 242–254. [CrossRef]
- 34. James, S.A.; Puttock, C.F.; Cordell, S.; Adams, R.P. Morphological and genetic variation within *Metrosideros polymorpha* (Myrtaceae) on Hawai'i. N. Z. J. Bot. **2004**, 42, 263–270. [CrossRef]
- 35. Izuno, A.; Kitayama, K.; Onoda, Y.; Tsujii, Y.; Hatakeyama, M.; Nagano, A.J.; Honjo, M.N.; Shimizu-Inatsugi, R.; Kudoh, H.; Shimizu, K.K.; et al. The population genomic signature of environmental association and gene flow in an ecologically divergent tree species *Metrosideros polymorpha* (Myrtaceae). *Mol. Ecol.* 2017, 26, 1515–1532. [CrossRef]
- 36. Stacy, E.A.; Johansen, J.B.; Sakishima, T.; Price, D.K. Genetic analysis of an ephemeral intraspecific hybrid zone in the hypervariable tree, *Metrosideros polymorpha*, on Hawai'i Island. *Heredity* **2016**, 117, 173–183. [CrossRef]
- 37. Joel, G.; Aplet, G.; Vitousek, P.M. Leaf Morphology Along Environmental Gradients in Hawaiian *Metrosideros polymorpha*. *Biotropica* **1994**, 26, 17–22. [CrossRef]
- 38. Martin, R.E.; Asner, G.P. Leaf Chemical and Optical Properties of *Metrosideros polymorpha* across Environmental Gradients in Hawaii. *Biotropica* **2009**, *41*, 292–301. [CrossRef]
- 39. Cordell, S.; Goldstein, G.; Mueller-Dombois, D.; Webb, D.; Vitousek, P.M. Physiological and morphological variation in *Metrosideros polymorpha*, a dominant Hawaiian tree species, along an altitudinal gradient: The role of phenotypic plasticity. *Oecologia* **1998**, 113, 188–196. [CrossRef] [PubMed]
- 40. Fisher, J.B.; Goldstein, G.; Jones, T.J.; Cordell, S. Wood vessel diameter is related to elevation and genotype in the Hawaiian tree *Metrosideros polymorpha* (Myrtaceae). *Am. J. Bot.* **2007**, *94*, 709–715. [CrossRef] [PubMed]
- 41. Tsujii, Y.; Onoda, Y.; Izuno, A.; Isagi, Y.; Kitayama, K. A quantitative analysis of phenotypic variations of *Metrosideros polymorpha* within and across populations along environmental gradients on Mauna Loa, Hawaii. *Oecologia* **2016**, *180*, 1049–1059. [CrossRef]
- 42. Cordell, S.; Goldstein, G.; Meinzer, F.C.; Handley, L.L. Allocation of nitrogen and carbon in leaves of *Metrosideros polymorpha* regulates carboxylation capacity and δ13C along an altitudinal gradient. *Funct. Ecol.* **1999**, *13*, 811–818. [CrossRef]
- 43. Choi, J.Y.; Purugganan, M.; Stacy, E.A. Divergent Selection and Primary Gene Flow Shape Incipient Speciation of a Riparian Tree on Hawaii Island. *Mol. Biol. Evol.* **2020**, *37*, 695–710. [CrossRef] [PubMed]
- 44. Kitayama, K.; Pattison, R.; Cordell, S.; Webb, D.; Mueller-dombois, D. Ecological and Genetic Implications of Foliar Polymorphism in *Metrosideros polymorpha*Gaud. (Myrtaceae) in a Habitat Matrix on Mauna Loa, Hawaii. *Ann. Bot.* 1997, 80, 491–497. [CrossRef]
- 45. Stacy, E.A.; Sakishima, T. Phylogeography of the highly dispersible landscape-dominant woody species complex, Metrosideros, in Hawaii. *J. Biogeogr.* **2019**, *46*, 2215–2231. [CrossRef]
- 46. Blonder, B.; Graae, B.J.; Greer, B.; Haagsma, M.; Helsen, K.; Kapás, R.E.; Pai, H.; Rieksta, J.; Sapena, D.; Still, C.J.; et al. Remote sensing of ploidy level in quaking aspen (Populus tremuloides Michx.). *J. Ecol.* **2020**, *108*, 175–188. [CrossRef]

Remote Sens. 2023, 15, 1614 17 of 18

47. Cavender-Bares, J.; Meireles, J.E.; Couture, J.J.; Kaproth, M.A.; Kingdon, C.C.; Singh, A.; Serbin, S.P.; Center, A.; Zuniga, E.; Pilz, G.; et al. Associations of Leaf Spectra with Genetic and Phylogenetic Variation in Oaks: Prospects for Remote Detection of Biodiversity. *Remote Sens.* 2016, 8, 221. [CrossRef]

- 48. Madritch, M.D.; Kingdon, C.C.; Singh, A.; Mock, K.E.; Lindroth, R.L.; Townsend, P.A. Imaging spectroscopy links aspen genotype with below-ground processes at landscape scales. *Philos. Trans. R. Soc. B Biol. Sci.* **2014**, *369*, 194. [CrossRef]
- 49. Sherrod, D.R.; Sinton, J.M.; Watkins, S.E.; Brunt, K.M. Geologic Map of the State of Hawai'i: U.S. Geologica Survey Open-File Report. 2007; p. 1089. Available online: http://pubs.usgs.gov/of/2007/1089/ (accessed on 4 January 2023).
- 50. Asner, G.P.; Knapp, D.E.; Boardman, J.; Green, R.O.; Kennedy-Bowdoin, T.; Eastwood, M.; Martin, R.E.; Anderson, C.; Field, C.B. Carnegie Airborne Observatory-2: Increasing science data dimensionality via high-fidelity multi-sensor fusion. *Remote Sens. Environ.* **2012**, 124, 454–465. [CrossRef]
- 51. Schaepman-Strub, G.; Schaepman, M.; Martonchik, J.; Schaaf, C. Whats in a Satellite Albedo Product? *IEEE Int. Symp. Geosci. Remote Sens.* **2006**, *6*, 2848–2852.
- 52. Miller, C.J. Performance assessment of ACORN atmospheric correction algorithm. In Proceedings of the Algorithms and Technologies for Multispectral, Hyperspectral, and Ultraspectral Imagery VIII, SPIE 2002, Melbourne, Australia, 16–18 December 2002; Volume 4725, pp. 438–449.
- 53. Asner, G.P.; Knapp, D.E.; Kennedy-Bowdoin, T.; Jones, M.O.; Martin, R.E.; Boardman, J.W.; Field, C.B. Carnegie Airborne Observatory: In-flight fusion of hyperspectral imaging and waveform light detection and ranging for three-dimensional studies of ecosystems. *J. Appl. Remote Sens.* **2007**, *1*, 013536. [CrossRef]
- 54. Feilhauer, H.; Asner, G.P.; Martin, R.E.; Schmidtlein, S. Brightness-normalized Partial Least Squares Regression for hyperspectral data. *J. Quant. Spectrosc. Radiat. Transf.* **2010**, *111*, 1947–1957. [CrossRef]
- 55. Curran, P.J.; Dungan, J.L.; Macler, B.A.; Plummer, S.E.; Peterson, D.L. Reflectance spectroscopy of fresh whole leaves for the estimation of chemical concentration. *Remote Sens. Environ.* **1992**, *39*, 153–166. [CrossRef]
- 56. Ustin, S.L.; Roberts, D.A.; Gamon, J.A.; Asner, G.P.; Green, R.O. Using Imaging Spectroscopy to Study Ecosystem Processes and Properties. *BioScience* **2004**, *54*, 523–534. [CrossRef]
- 57. Wang, R.; Gamon, J.A.; Cavender-Bares, J.; Townsend, P.A.; Zygielbaum, A.I. The spatial sensitivity of the spectral diversity—biodiversity relationship: An experimental test in a prairie grassland. *Ecol. Appl.* **2018**, *28*, 541–556. [CrossRef]
- 58. Thompson, D.R.; Boardman, J.W.; Eastwood, M.L.; Green, R.O. A large airborne survey of Earth's visible-infrared spectral dimensionality. *Opt. Express* **2017**, 25, 9186. [CrossRef] [PubMed]
- 59. Boardman, J.W.; Green, R.O. Exploring the spectral variability of the Earth as measured by AVIRIS in 1999. Summaries of the ninth annual JPL airborne geosciences workshop. *Jet Propuls. Lab. Spec. Publ.* **2000**, *18*, 10.
- 60. Green, R.O.; Boardman, J.W. Exploration of the relationship between information content and signal-to-noise ratio and spatial resolution in AVIRIS spectral data. *Spectrum* **2000**, *7*, 8.
- 61. Dai, J.; Vaughn, N.R.; Seeley, M.; Heckler, J.; Thompson, D.R.; Asner, G.P. Spectral dimensionality of imaging spectroscopy data over diverse landscapes and spatial resolutions. *J. Appl. Remote Sens.* **2022**, *16*, 044518. [CrossRef]
- 62. Baldeck, C.A.; Colgan, M.S.; Féret, J.-B.; Levick, S.R.; Martin, R.E.; Asner, G.P. Landscape-scale variation in plant community composition of an African savanna from airborne species mapping. *Ecol. Appl.* **2014**, 24, 84–93. [CrossRef] [PubMed]
- 63. Baldeck, C.A.; Asner, G.P.; Martin, R.E.; Anderson, C.B.; Knapp, D.E.; Kellner, J.R.; Wright, S.J. Operational Tree Species Mapping in a Diverse Tropical Forest with Airborne Imaging Spectroscopy. *PLoS ONE* **2015**, *10*, e0118403. [CrossRef] [PubMed]
- 64. Balzotti, C.S.; Asner, G.P.; Adkins, E.D.; Parsons, E.W. Spatial drivers of composition and connectivity across endangered tropical dry forests. *J. Appl. Ecol.* **2020**, *57*, 1593–1604. [CrossRef]
- 65. Camps-Valls, G.; Gomez-Chova, L.; Calpe-Maravilla, J.; Martin-Guerrero, J.D.; Soria-Olivas, E.; Alonso-Chorda, L.; Moreno, J. Robust support vector method for hyperspectral data classification and knowledge discovery. *IEEE Trans. Geosci. Remote Sens.* **2004**, 42, 1530–1542. [CrossRef]
- 66. Feret, J.-B.; Asner, G.P. Tree Species Discrimination in Tropical Forests Using Airborne Imaging Spectroscopy. *IEEE Trans. Geosci. Remote Sens.* **2013**, *51*, *73*–84. [CrossRef]
- 67. Melgani, F.; Bruzzone, L. Classification of hyperspectral remote sensing images with support vector machines. *IEEE Trans. Geosci. Remote Sens.* **2004**, 42, 1778–1790. [CrossRef]
- 68. Pedregosa, F.; Varoquaux, G.; Gramfort, A.; Michel, V.; Thirion, B.; Grisel, O.; Blondel, M.; Prettenhofer, P.; Weiss, R.; Dubourg, V.; et al. Scikit-learn: Machine Learning in Python. *J. Mach. Learn. Res.* **2011**, *12*, 2825–2830.
- 69. Porder, S.; Asner, G.P.; Vitousek, P.M. Ground-based and remotely sensed nutrient availability across a tropical landscape. *Proc. Natl. Acad. Sci. USA* **2005**, *102*, 10909–10912. [CrossRef]
- 70. Balzotti, C.S.; Asner, G.P. Biotic and Abiotic Controls Over Canopy Function and Structure in Humid Hawaiian Forests. *Ecosystems* **2018**, *21*, 331–348. [CrossRef]
- 71. Corn, C.A.; Hiesey, W.M. Altitudinal Variation in Hawaiian Metrosideros. Am. J. Bot. 1973, 60, 991–1002. [CrossRef]
- 72. Drake, D.R.; Mueller-Dombois, D. Population Development of Rain Forest Trees on a Chronosequence of Hawaiian Lava Flows. *Ecology* **1993**, 74, 1012–1019. [CrossRef]
- 73. Stemmermann, L. Ecological studies of Hawaiian Metrosideros in a successional context. Pac. Sci. 1983, 37, 361–373.
- 74. Poorter, H.; Niinemets, Ü.; Poorter, L.; Wright, I.J.; Villar, R. Causes and consequences of variation in leaf mass per area (LMA): A meta-analysis. *New Phytol.* **2009**, *182*, 565–588. [CrossRef]

Remote Sens. 2023, 15, 1614 18 of 18

75. Westoby, M.; Falster, D.; Moles, A.T.; Vesk, P.; Wright, I.J. Plant Ecological Strategies: Some Leading Dimensions of Variation Between Species. *Annu. Rev. Ecol. Syst.* **2002**, *33*, 125–159. [CrossRef]

- 76. Wright, S.J.; Kitajima, K.; Kraft, N.J.B.; Reich, P.B.; Wright, I.J.; Bunker, D.E.; Condit, R.; Dalling, J.W.; Davies, S.J.; Díaz, S.; et al. Functional traits and the growth–mortality trade-off in tropical trees. *Ecology* **2010**, *91*, 3664–3674. [CrossRef] [PubMed]
- 77. Crews, T.E.; Kitayama, K.; Fownes, J.H.; Riley, R.H.; Herbert, D.A.; Mueller-Dombois, D.; Vitousek, P.M. Changes in Soil Phosphorus Fractions and Ecosystem Dynamics across a Long Chronosequence in Hawaii. *Ecology* **1995**, *76*, 1407–1424. [CrossRef]
- 78. Vitousek, P.M.; Matson, P.A.; Turner, D.R. Elevational and age gradients in hawaiian montane rainforest: Foliar and soil nutrients. *Oecologia* 1988, 77, 565–570. [CrossRef]
- 79. Hoof, J.; Sack, L.; Webb, D.T.; Nilsen, E.T. Contrasting Structure and Function of Pubescent and Glabrous Varieties of Hawaiian *Metrosideros polymorpha* (Myrtaceae) at High Elevation. *Biotropica* **2008**, 40, 113–118. [CrossRef]
- 80. Kitayama, K.; Mueller-Dombois, D. Vegetation changes along gradients of long-term soil development in the Hawaiian montane rainforest zone. *Vegetatio* **1995**, *120*, 1–20. [CrossRef]
- 81. Stacy, E.; Johnson, M. Floral Variation across Three Varieties of the Landscape-Dominant Tree *Metrosideros polymorpha* (Myrtaceae): Insights from a Hawaii Island Common Garden. *Int. J. Plant Sci.* **2021**, *182*, 46–58. [CrossRef]
- 82. Ustin, S.L.; Riaño, D.; Hunt, E.R. Estimating canopy water content from spectroscopy. Isr. J. Plant Sci. 2012, 60, 9–23. [CrossRef]
- 83. Townsend, P.A.; Foster, J.R.; Chastain, R.A.; Currie, W.S. Application of imaging spectroscopy to mapping canopy nitrogen in the forests of the central Appalachian Mountains using Hyperion and AVIRIS. *IEEE Trans. Geosci. Remote Sens.* **2003**, *41*, 1347–1354. [CrossRef]

Disclaimer/Publisher's Note: The statements, opinions and data contained in all publications are solely those of the individual author(s) and contributor(s) and not of MDPI and/or the editor(s). MDPI and/or the editor(s) disclaim responsibility for any injury to people or property resulting from any ideas, methods, instructions or products referred to in the content.